Glacial to Holocene swings of the Australian-Indonesian monsoon

Mahyar Mohtadi[1*], Delia W. Oppo[2], Stephan Steinke[1], Jan-Berend W. Stuut[1,3], Ricardo De Pol-Holz[4,5], Dierk Hebbeln[1], Andreas Lückge[6]

[1] *Center for Marine Environmental Sciences (MARUM), University of Bremen, 28359 Bremen, Germany*

[2] *Geology & Geophysics, Woods Hole Oceanographic Institution (WHOI), Woods Hole, MA 02543, USA*

[3] *Royal Netherlands Institute for Sea Research (NIOZ), NL-1790 AB, Texel, The Netherlands*

[4] *Earth System Science Department, University of California, Irvine, CA 92697, USA*

[5] *Department of Oceanography, Universidad de Concepción, Concepción, Chile*

[6] *Federal Institute for Geosciences and Natural Resources (BGR), 30655 Hannover, Germany*

[*]e-mail: mohtadi@uni-bremen.de

The Australian-Indonesian monsoon is an important component of the climate system in the tropical Indo-Pacific region[1]. However, its past variability, relation with northern and southern high latitude climate and connection to the other Asian monsoon systems are poorly understood. Here we present high-resolution records of monsoon-controlled austral winter upwelling during the past 22,000 years, based on planktic foraminiferal oxygen isotope and faunal composition in a sedimentary archive collected offshore southern Java. We show that glacial-interglacial variations in the Australian-Indonesian winter monsoon were in phase with the Indian summer monsoon system, consistent with their modern linkage through cross-equatorial surface winds. Likewise, millennial-scale variability of upwelling shares similar sign and timing with upwelling variability in the Arabian Sea. On the basis of element composition and grain-size distribution as precipitation-sensitive proxies in the same archive, we infer that (austral) summer monsoon rainfall was highest during the Bølling-Allerød period and the past 2,500 years. Our results indicate drier conditions during Heinrich Stadial 1 due to a southward shift of summer rainfall and a relatively weak Hadley Cell south of the Equator. We suggest that the Australian-Indonesian summer and winter monsoon variability were closely linked to summer insolation and abrupt climate changes in the northern hemisphere.

The seasonality of the global monsoon is of central importance to the global hydrologic cycle and its environmental influence on human societies. Paleoclimate reconstructions generally agree that the strength of the East Asian monsoon and the Indian monsoon are tightly coupled to the Northern Hemisphere climate through zonal migrations of the monsoon convection centers, also interpreted as Intertropical Convergence Zone (ITCZ) migration[2-6]. The mechanism of the Australian-Indonesian monsoon (AIM) in both time and space is, however, poorly understood[7-12]. Australian records[9-11] indicate wetter-than-today conditions during the early and middle Holocene. These changes have been explained through

a Northern Hemisphere insolation control on the AIM (refs 8,10), regional sea surface temperature (SST) feedback[7] or human impact on the late Holocene vegetation cover[8], countering or even canceling the response of the AIM to local insolation. Deglacial sea level rise and its effect on exposed land surface may also be an important influence on southeast Indonesian rainfall[12,13]. Moreover, many records suggest that the Asian monsoons, including the AIM, changed in association with North Atlantic deglacial climate oscillations that were accompanied by variations in the Atlantic Meridional Overturning Circulation (AMOC; erfs 3,10,14). Further records of the AIM, especially those that reflect a known season, are needed to understand how these various possible influences affect the AIM.

Here we present high-resolution paleoclimatic records from sediment core GeoB 10053-7 collected off South Java (8°41´ S, 112°52’ E, 1375 m water depth, Fig. 1) that span the past 22,000 years. At present, the seasonal migration of the coupled monsoon-ITCZ systems governs the seasonal climate variability at the core site. During austral summer (henceforth summer), the northwest monsoon gathers large amounts of moisture while crossing sea from the Asian high-pressure belt on its way to the ITCZ. Maximum rainfall reaches the study area, including eastern Indonesia and Australia, in January (Fig. 1). During austral winter (henceforth winter), the southeast monsoon originates from the Southern Hemisphere high-pressure belt and the study area is relatively dry and cool. Ekman transport and coastal upwelling in the study area peak between July and September (see Supplementary Information).

Our paleoclimate time series resolve both seasonal signals of the AIM in the same, continuous sedimentary archive over the past 22,000 years. We use *G. bulloides* percentages as a proxy for winter upwelling and monsoon intensity. Our results suggest that upwelling off Java, and thus the Australian-Indonesian winter monsoon (AIWM), was weakest during the Last Glacial Maximum (LGM) and the late Holocene, and strongest during the early Holocene. These trends are paralleled by trends in the difference in $\delta^{18}O$ of calcite between

the annual-mean and winter ($\Delta\delta^{18}O$), whereby greater differences imply stronger upwelling and intensified AIWM (Fig. 2c, see Supplementary Information). Differences between these upwelling-sensitive records are likely due to the additional and different influences of temperature on the individual $\delta^{18}O$ records. Similar upwelling trends in the Arabian Sea[14] (Fig 2e) during the same season (that is boreal summer and austral winter) indicate that these upwelling systems changed together, and provide strong evidence that they reflect variations in the strength of large-scale cross-equatorial boreal summer-austral winter monsoon winds, probably in response to Northern Hemisphere summer insolation[7,15] (Fig. 2d). This inference should be explored further with AIWM records that span several glacial-interglacial cycles.

Superimposed on the long-term variability of the Java upwelling are a number of deglacial AIWM variations of millennial-scale duration, that are best expressed in the percentage of *G. bulloides*. Although these variations are relatively subtle, similar features are recorded in the upwelling record from the Arabian Sea[14], suggesting that they reflect large-scale changes in southerly cross-equatorial winds. For example, the relative contribution of *G. bulloides* of both regions (Figs. 2d,e) suggest modestly higher upwelling during the Heinrich Stadial 1 period (HS 1) that deteriorated to near glacial values during the Bølling-Allerød period (B-A), followed by intensified upwelling during the Younger Dryas period (YD). The coincident timing of the observed millennial-scale oscillations in the upwelling area off South Java and the Arabian Sea during the last deglaciation indicates that changes in the AIWM intensity were closely linked to the Indian monsoon. Moreover, these millennial oscillations are closely related to abrupt climate changes in the North Atlantic region (Fig. 2a). We note that a significantly larger surface reservoir age than used here (see Supplementary Information) might align these abrupt events better with North Atlantic events. A better alignment of these events with the onset of Southern Hemisphere climate at 18,000 years ago (for example Fig. 2g) and the end of the Antarctic Cold Reversal would require a less-than-zero surface-reservoir age.

Proxy records for runoff also enable us to evaluate changes in the Australian-Indonesian summer monsoon (AISM). In contrast to the AIWM, there is little evidence for large LGM-Holocene trends in AISM, with only Ti/Ca ratios suggesting that the Holocene was slightly wetter than the LGM and early deglacial (HS 1). This trend, although small, is consistent with the opposite evolution of the boreal winter monsoon in the Northern Hemisphere[16], as recorded in Chinese loess sediments (Fig. 3e). Instead, millennial-scale oscillations dominate the records. The terrigenous fraction of the sediment indicates higher continental runoff caused by stronger AISM rainfall during the B-A and the past 2,500 years (Fig. 3b-c). In contrast, the LGM, HS 1 and YD are characterized by the lowest continental runoff due to a less intense AISM. The grain-size distribution of the terrigenous fraction in 112 selected samples further supports these findings (Fig. 3d, Supplementary Information). Sediments deposited during the HS 1 and YD are characterized by a lower terrigenous content that is coarser than during the remaining periods, suggesting a predominantly eolian source of the terrigenous sediment fraction, possibly transported from the interior of Australia. Conversely, sediments deposited during the B-A and the late Holocene contain more fine terrigenous components, suggestive of increased continental runoff and a dominant fluvial source of the terrigenous fraction due to increased AISM rainfall. In summary, our proxy data from south of Java show a strong (wet) AISM during the B-A and the late Holocene, and a weak (dry) AISM during HS 1 and the YD, indicating that the AISM intensity was also closely linked to the Northern Hemisphere abrupt climate changes during the last deglaciation (Fig. 3a-c).

Our inferences of AISM and AIWM millennial variability are not entirely consistent with the interpretation of speleothem $\delta^{18}O$ records from the East Asian monsoon and AIM regions, which may vary owing to a number of processes[17,18]. Chinese speleothem records have generally been interpreted to reflect changes in the relative strengths of the East Asian boreal summer and winter monsoon (EAWM and EASM) intensities, and suggest a relatively

weak EASM during HS 1 and the YD and a relatively strong EASM during the B-A (ref. 3; Fig. 2f). The opposite developments of the AIWM and EASM during these periods (Fig. 2) is surprising, given that the AIWM winds at present 'feed' the EASM through cross-equatorial winds (Fig. 1). It is possible that millennial-scale variations in the $\delta^{18}O$ of precipitation over coastal China reflect changes in the source of precipitation and the influence of upwind hydrologic non-local changes in the amount effect, as suggested by recent modeling studies[18], and these changes are decoupled from cross-equatorial winds.

Our sedimentary evidence of AISM variability, suggesting drier conditions during HS 1 and wetter conditions during most of the B-A, are consistent with speleothem $\delta^{18}O$ records from northwestern Borneo[13] (Fig. 3f). Together with records from Lynch's Crater in northeastern Australia, which show increased moisture during HS 1(refs 19,20), they suggest a southerly position of the austral summer ITCZ compared with the present. Although drying during HS 1 inferred from our records and the Borneo $\delta^{18}O$ record is consistent with a large decrease in local rainfall during dramatic AMOC events such as HS 1 (ref. 18), the evidence for the YD is more complex. Whereas our records suggest a weaker AISM (drying) during the YD, speleothem records from both Borneo and Flores[12] imply a return to wetter conditions during the YD (Fig. 3f,g). These differences may imply that the mechanisms causing $\delta^{18}O$ changes in precipitation of the region are more complex during times of modest AMOC reduction, or that there were sharp northeast-to-southwest gradients in precipitation within Indonesia. Simulations of the rainfall variability over the Indo-Pacific Warm Pool suggest an eastward displacement of the Walker and Hadley Circulations during the LGM (ref. 21), and a weakened and easterly displaced Hadley Circulation in the southern part of the Indo-Pacific Warm Pool during HS 1 and the YD in response to a weak AMOC (ref. 22). Although boundary conditions during the LGM and deglaciation were not considered in these simulations, these results suggest that weaker and easterly displaced convection centers might have caused the dry conditions observed in our proxy records during the LGM, HS 1 and YD.

It should be noted that the timing of deglacial millennial-scale variability discussed above is subject to uncertainties in our age model (as discussed in Supplementary Information). Although future work in the Java upwelling area should attempt to describe reservoir age changes through time, it is unlikely that age discrepancies alone account for differences in interpretation between our records and the published speleothem records from this region.

The Holocene evolution of the AISM rainfall in our records, a drier early and middle Holocene compared with the late Holocene (Fig. 3), differ with evidence from the Indo-Pacific Warm Pool records, whereas Australian lake sediments[9-11] indicate conditions wetter than today during the early and middle Holocene. One possible explanation for the difference in timing between Australia and Flores/Java is the northward shift of austral summer precipitation (ITCZ). In this scenario, the earlier maximum in Borneo than Flores/Java may be because it reflects both summer and winter precipitation[12]. Alternative explanations for the different trends include changes in boundary conditions over the Australian landmass[7,8]. More data and modeling experiments are needed to identify the most important mechanisms for these different trends.

Our results clearly indicate similar long-term variations of the AIWM wind and the EASM rainfall, probably due to their common forcing by Northern Hemisphere summer insolation. Glacial-interglacial AISM rainfall changes are small, but negatively correlated to the EAWM, as expected from north-to-south ITCZ migrations. On millennial timescales, however, variations in AIWM winds are not in agreement with interpretations of Chinese speleothem $\delta^{18}O$ records as reflecting variations in the seasonality of precipitation, consistent with modelling evidence that the $\delta^{18}O$ of East Asian monsoon precipitation in response to abrupt AMOC events is controlled by other mechanisms, which will have to be explored further in future studies. Our results confirm a spatially coherent drying pattern throughout Indonesia due to southerly displaced ITCZ during the strong AMOC reduction of HS 1. However, our evidence of reduced runoff during the YD contrasts with Indonesian

speleothem evidence of wetter conditions, suggesting either that mechanisms other than enhanced rainfall influenced speleothem $\delta^{18}O$, or that there were sharp precipitation gradients in Indonesia at this time. Sediment-age model uncertainties, which may lead to some of these discrepancies on millennial time scales, will also have to be explored in future studies.

Methods

The age model is based on 19 radiocarbon dates yielding average sedimentation rates of 37 cm kyr^{-1} (see Supplementary Information). We analysed the stable oxygen isotope ($\delta^{18}O$) composition in calcite shells of the surface-dwelling planktic foraminifera *G. ruber* sensu stricto and *G. bulloides* in 290 samples, achieving an average temporal resolution of 75 years per sample. Modern observations from the study area show that *G. ruber* reflects annual-mean surface conditions, whereas *G. bulloides* records surface conditions during the winter AIM (ref. 23; AIWM, June-October), when coastal upwelling occurs (see Supplementary Information). We calculated the abundance of *G. bulloides* relative to total planktic foraminiferal fauna as a measure of past changes in upwelling intensity. In this context, higher values of *G. bulloides* are interpreted as intensified upwelling caused by a stronger winter monsoon.

We also carried out element analyses using the X-ray fluorescence method, and calculated the lithogenic fraction of sediment. Variations in the Ti/Ca ratio determined by X-ray fluorescence and in the lithogenic/$CaCO_3$ ratio from the bulk sediment analysis show a strong correlation throughout the entire record (Fig. 3). On the basis of modern observations, these ratios represent continental runoff that is controlled by the summer AIM (AISM, December-March) precipitation, with higher ratios reflecting enhanced runoff and a stronger AISM (see Supplementary Information). Median grain size, measured with laser particle

sizer, provides a qualitative measure for the source of the terrigenous components, with smaller size indicating more fluvial delivery and larger sizes indicating more eolian delivery.

References

1 Webster, P. J. *et al.* Monsoons: Processes, predictability, and the prospects for prediction. *Journal of Geophysical Research* **103**, 14,451-414,510 (1998).

2 Wang, Y. *et al.* The Holocene Asian Monsoon: Links to Solar Changes and North Atlantic Climate. *Science* **308**, 854-857, doi:10.1126/science.1106296 (2005).

3 Wang, Y. J. *et al.* A high-resolution absolute-dated Late Pleistocene monsoon record from Hulu Cave, China. *Science* **294**, 2345-2348, doi:10.1126/science.1064618 (2001).

4 Chao, W. C. & Chen, B. The Origin of Monsoons. *Journal of the Atmospheric Sciences* **58**, 3497-3507 (2001).

5 Wang, P. Global monsoon in a geological perspective. *Chinese Science Bulletin* **54**, 1113-1136 (2009).

6 Gupta, A. K., Anderson, D. M. & Overpeck, J. T. Abrupt changes in the Asian southwest monsoon during the Holocene and their links to the North Atlantic Ocean. *Nature* **421**, 354-357 (2003).

7 Liu, Z., Otto-Bliesner, B., Kutzbach, J., Li, L. & Shields, C. Coupled Climate Simulation of the Evolution of Global Monsoons in the Holocene. *Journal of Climate* **16**, 2472-2490 (2003).

8 Miller, G. *et al.* Sensitivity of the Australian Monsoon to insolation and vegetation: Implications for human impact on continental moisture balance. *Geology* **33**, 65-68, doi:10.1130/g21033.1 (2005).

9 Johnson, B. J. *et al.* 65,000 years of vegetation change in central Australia and the Australian summer monsoon. *Science* **284**, 1150-1152 (1999).

10 Magee, J. W., Miller, G. H., Spooner, N. A. & Questiaux, D. Continuous 150 k.y. monsoon record from Lake Eyre, Australia: Insolation-forcing implications and unexpected Holocene failure. *Geology* **32**, 885-888, doi:10.1130/g20672.1 (2004).

11 Nott, J. & Price, D. Plunge pools and paleoprecipitation. *Geology* **22**, 1047-1050, doi:10.1130/0091-7613 (1994).

12 Griffiths, M. L. *et al.* Increasing Australian-Indonesian monsoon rainfall linked to early Holocene sea-level rise. *Nature Geoscience* **2**, 636-639 (2009).

13 Partin, J. W., Cobb, K. M., Adkins, J. F., Clark, B. & Fernandez, D. P. Millennial-scale trends in west Pacific warm pool hydrology since the Last Glacial Maximum. *Nature* **449**, 452-455 (2007).

14 Naidu, P. D. & Malmgren, B. A. A High-resolution record of Late Quaternary upwelling along the Oman Margin, Arabian Sea based on planktonic foraminifera. *Paleoceanography* **11**, 129-140, doi:doi:10.1029/95PA03198 (1996).

15 Kutzbach, J. E. Monsoon climate of the Early Holocene: climate experiment with the Earth's orbital parameters for 9000 years ago. *Science* **214**, 59-61 (1981).

16 Sun, Y., Clemens, S. C., An, Z. & Yu, Z. Astronomical timescale and palaeoclimatic implication of stacked 3.6-Myr monsoon records from the Chinese Loess Plateau. *Quaternary Science Reviews* **25**, 33-48 (2006).

17 Clemens, S. C., Prell, W. L. & Sun, Y. Orbital-scale timing and mechanisms driving Late Pleistocene Indo-Asian summer monsoons: Reinterpreting cave speleothem $\delta^{18}O$. *Paleoceanography* **25**, PA4207, doi:10.1029/2010pa001926 (2010).

18 Lewis, S. C., LeGrande, A. N., Kelley, M. & Schmidt, G. A. Water vapour source impacts on oxygen isotope variability in tropical precipitation during Heinrich events. *Climate of the Past Discussions* **6**, 87-133 (2010).

19 Turney, C. S. M. *et al.* Millennial and orbital variations of El Niño/Southern Oscillation and high-latitude climate in the last glacial period. *Nature* **428**, 306-310 (2004).

20 Muller, J. *et al.* Possible evidence for wet Heinrich phases in tropical NE Australia: the Lynch's Crater deposit. *Quaternary Science Reviews* **27**, 468-475 (2008).

21 Kitoh, A. & Murakami, S. Tropical Pacific climate at the mid-Holocene and the Last Glacial Maximum simulated by a coupled ocean-atmosphere general circulation model. *Paleoceanography* **17**, 1047, doi:1010.1029/2001PA000724 (2002).

22 Zhang, R. & Delworth, T. L. Simulated Tropical Response to a Substantial Weakening of the Atlantic Thermohaline Circulation. *Journal of Climate* **18**, 1853-1860 (2005).

23 Mohtadi, M. *et al.* Low-latitude control on seasonal and interannual changes in planktonic foraminiferal flux and shell geochemistry off south Java: A sediment trap study. *Paleoceanography* **24**, PA1201, doi:1210.1029/2008PA001636 (2009).

24 Qu, T., Du, Y., Strachan, J., Meyers, G. & Slingo, J. M. Sea surface temperature and its variability in the Indonesian region. *Oceanography* **18**, 50-62 (2005).

25 Grootes, P. M. & Stuiver, M. Oxygen 18/16 variability in Greenland snow and ice with 10^{-3} to 10^{5}-year time resolution. *Journal of Geophysical Research* **102 No. C12**, 26,455-426,470 (1997).

26 Wang, Y. *et al.* Millennial- and orbital-scale changes in the East Asian monsoon over the past 224,000 years. *Nature* **451**, 1090-1093 (2008).

27 Stenni, B. *et al.* A late-glacial high-resolution site and source temperature record derived from the EPICA Dome C isotope records (East Antarctica). *Earth and Planetary Science Letters* **217**, 183-195 (2004).

Acknowledgements

We are grateful to M. Segl, B. Meyer-Schack, M. Klann, H. Buschoff, V. Lukies, and I. Meyer for technical support. This study was funded by the German Bundesministerium für Bildung und Forschung (PABESIA) and the Deutsche Forschungsgemeinschaft (DFG, HE 3412/15-1). DWO's participation was funded by the U.S. National Science Foundation.

Author contributions

M.M. was responsible for oxygen isotopes analyses and *G. bulloides* counts, J-B.W.S. was responsible for the grain-size data, R.D. and D.W.O. were responsible for the radiocarbon analyses, M.M. and S.S. were responsible for the X-ray fluorescence and lithogenic data, D.H. was chief investigator and A.L. was partner investigator, M.M., D.W.O. and S.S. wrote the paper; all the authors discussed the paper.

Additional information

The authors declare no competing financial interests. Supplementary information accompanies this paper on www.nature.com/naturegeoscience. Reprints and permissions information is available online at http://www.nature.com/reprints. Correspondence and requests for materials should be addressed to M.M.

Figure captions

Figure 1.

Monsoonal cyclicity in SST and wind trajectory in the tropical Indo-Pacific. a,**b**, The colour chart indicates seasonal SSTs for winter (**a**, July-September) and summer (**b**, January-March). Remote-sensing SST data are averaged from January 2002 to February 2008 (Aqua MODIS, http://oceancolor.gsfc.nasa.gov). Superimposed are quick scatterometer winds

(arrows) in August (**a**) and February (**b**; ref. 24). Wind data are averaged from December 1997 to June 2004 and from July 1999 to January 2005, respectively. The black circle indicates the position of the investigated core.

Figure 2.

Proxy records for the winter AIM and other palaeoclimate records over the past 22,000 years. a, $\delta^{18}O$ record of GISP 2 ice core (Greenland)[25]. **b**, $\delta^{18}O$ records of *Globigerinoides ruber* (black, annual mean) and *G. bulloides* (grey, winter, July-September) in core GeoB 10053-7 off southern Java. **c**, Their difference ($\Delta^{18}O$, blue), with a nine-point running average (thick dark-blue line). **d**, Relative contribution of *G. bulloides* (red) in the same core; superimposed is the June insolation at 30°N (black). **c** and **d** indicate changes in the upwelling intensity off southern Java that is controlled by the AIWM. **e**, Relative contribution of *G. bulloides* (green) in the Arabian Sea[14] indicative of changes in the Indian Summer Monsoon (ISM). **f**, Stacked $\delta^{18}O$ of stalagmites in Chinese caves[26] (pink) indicating changes in the EASM-related precipitation. **g**, $\delta^{18}O$ record of EPICA Dome C (EDC) ice core (East Antarctica, brown)[27]. Triangles denote radiocarbon datings; vertical bars correspond to the HS 1, B-A and YD periods, respectively. ACR, Antarctic Cold Reversal.

Figure 3.

Proxy records for the summer AIM and other palaeoclimate records over the past 22,000 years. a, $\delta^{18}O$ record of GISP 2 ice core (Greenland)[25]. **b**,**c**, Lithogenic/$CaCO_3$ (**b**, black) and Ti/Ca (**c**, grey) ratios in core GeoB 10053-7 off southern Java. Superimposed are Si/Al data (black dots) from Lynch's Crater[20]. **d**, Median grain size of the terrigenous fraction of the sediment (blue). **b-d** indicate changes in the amount (**b,c**) and composition (**d**) of the continental runoff that is controlled by the AISM. **e**, Stacked mean grain size of quartz in Chinese Loess Plateau[16] (red), indicative of changes in the EAWM intensity. **f**, Stacked $\delta^{18}O$ of speleothems in Borneo[13] (green). **g**, Stacked $\delta^{18}O$ of speleothems in Flores[12] (pink),

indicating changes in the AISM- and sea-level-related precipitation. **h**, $\delta^{18}O$ record of EPICA Dome C (EDC) ice core (East Antarctica, brown)[27]. Vertical bars, triangles and abbreviations are as in Fig. 2.

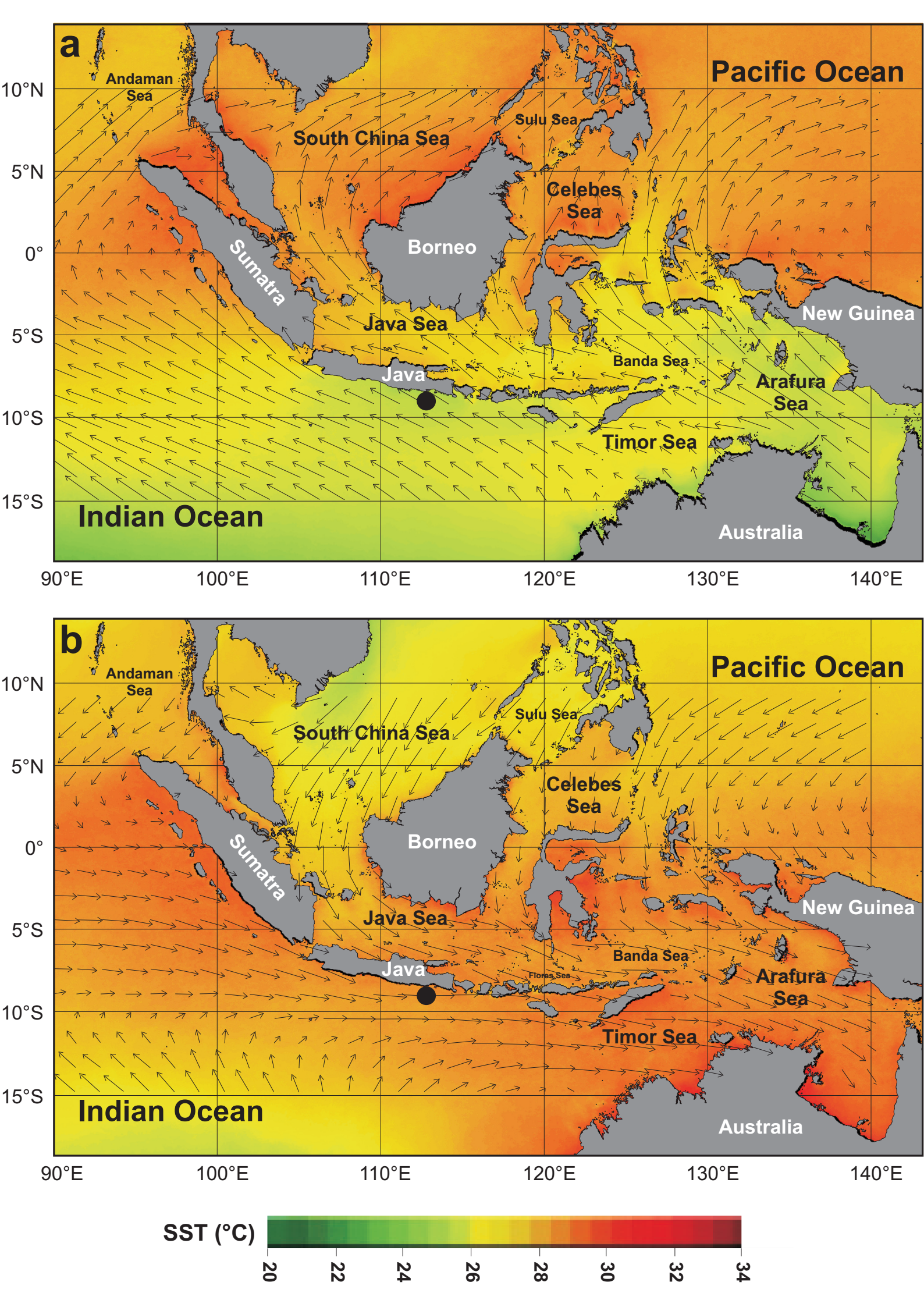
a
Andaman Sea
Pacific Ocean
South China Sea
Sulu Sea
Celebes Sea
Borneo
Sumatra
Java Sea
New Guinea
Banda Sea
Java
Arafura Sea
Timor Sea
Indian Ocean
Australia
10°N
5°N
0°
5°S
10°S
15°S
90°E
100°E
110°E
120°E
130°E
140°E
b
Andaman Sea
Pacific Ocean
Sulu Sea
South China Sea
Celebes Sea
Borneo
Sumatra
Java Sea
New Guinea
Banda Sea
Java
Flores Sea
Arafura Sea
Timor Sea
Indian Ocean
Australia
10°N
5°N
0°
5°S
10°S
15°S
90°E
100°E
110°E
120°E
130°E
140°E
SST (°C)
20
22
24
26
28
30
32
34

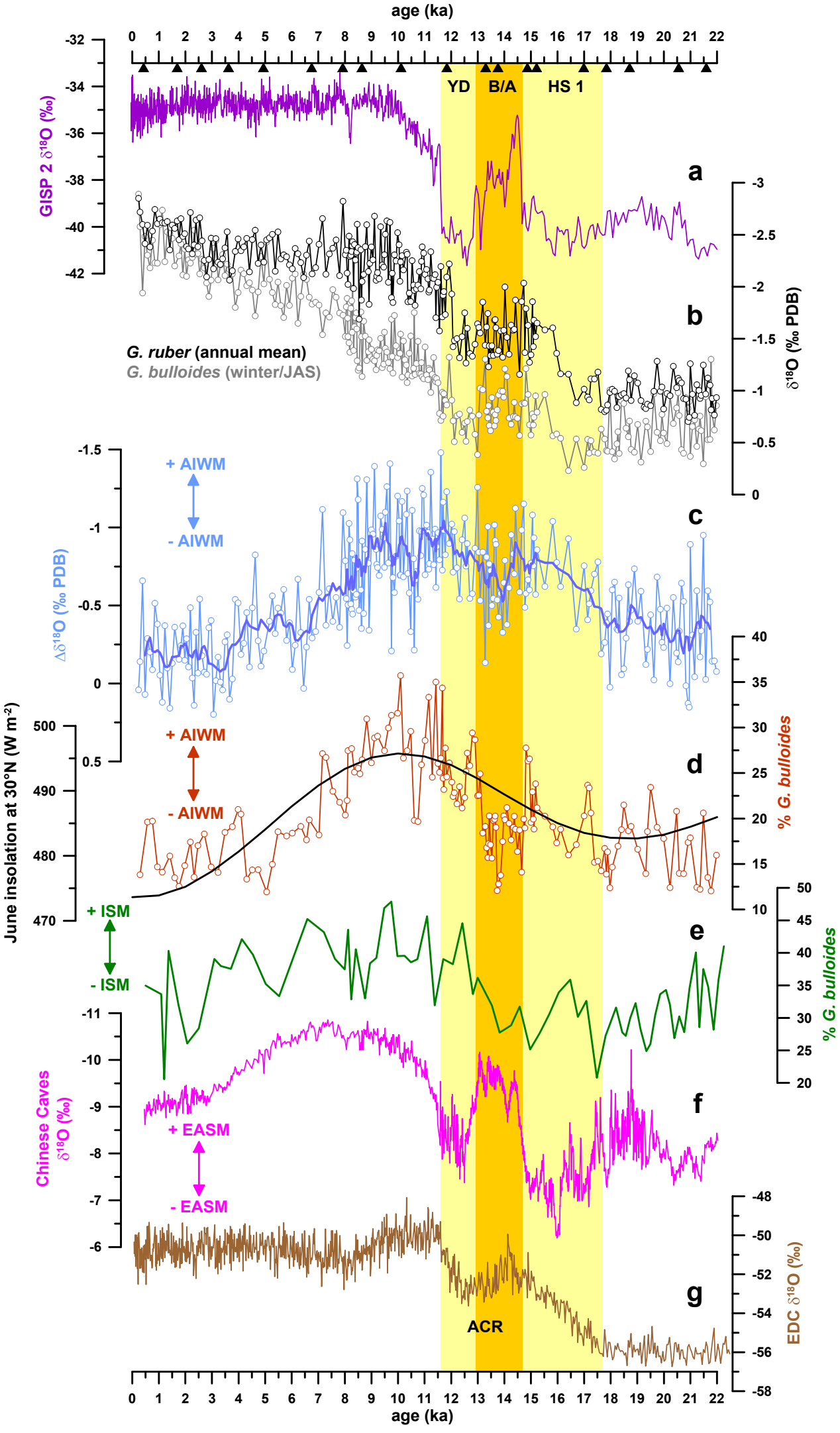
age (ka)
YD
B/A
HS 1
GISP 2 δ18O (‰)
a
b
G. ruber (annual mean)
G. bulloides (winter/JAS)
δ18O (‰ PDB)
+ AIWM
- AIWM
Δδ18O (‰ PDB)
c
June insolation at 30°N (W m-2)
+ AIWM
- AIWM
d
% G. bulloides
+ ISM
- ISM
e
% G. bulloides
Chinese Caves δ18O (‰)
+ EASM
- EASM
f
ACR
g
EDC δ18O (‰)
age (ka)

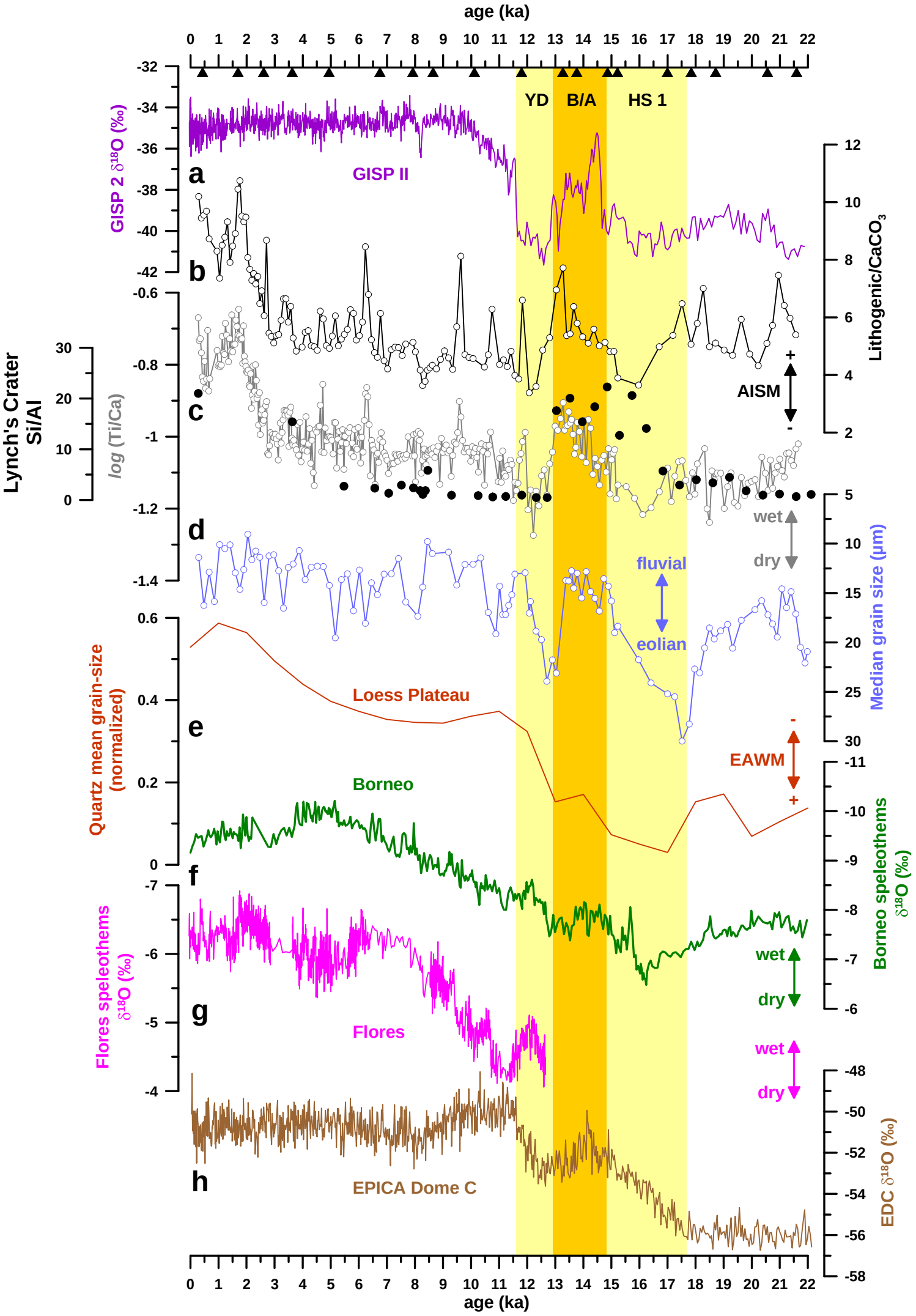
age (ka)
YD
B/A
HS 1
GISP 2 δ18O (‰)
GISP II
a
b
c
d
e
f
g
h
Lithogenic/CaCO3
AISM
+
-
Lynch's Crater Si/Al
log (Ti/Ca)
wet
dry
fluvial
eolian
Median grain size (μm)
Quartz mean grain-size (normalized)
Loess Plateau
EAWM
Borneo
Borneo speleothems δ18O (‰)
Flores speleothems δ18O (‰)
Flores
EPICA Dome C
EDC δ18O (‰)

Supplementary Information – Glacial to Holocene swings of the Australian-Indonesian monsoon by Mohtadi et al.

Sampling

Sediment core GeoB 10053-7 (8° 40.59´S, 112° 52.35´ E, 1375m water depth, 750 cm core length) was collected off south Java during the *SO-184* "PABESIA" expedition. For foraminiferal and bulk sediment analyses, the core was cut and sub-sampled at 5 cm steps onboard *R/V Sonne*[1]. The bottom 350 cm of the core was additionally sampled at 2 cm steps for planktonic foraminiferal analyses. The core depth lies more than 800 m above the present-day calcite lysocline (>2200 m)[2], and well-preserved pteropods are present throughout the core. We therefore exclude any significant altering of the primary signal of the planktonic foraminifera shell chemistry by calcite dissolution.

Age model

The age model is based on 19 accelerator mass spectrometry (AMS) ^{14}C dates and the linear interpolation between them (Table S1, Fig. S1). AMS dating was performed at the National Ocean Sciences Accelerator Mass Spectrometry Facility (NOSAMS) in Woods Hole, USA, and at Keck Carbon Cycle Accelerator Mass Spectrometry Laboratory (KCCAMS) in Irvine, USA. AMS ^{14}C dates were obtained on 9-20 mg calcium carbonate from mixed planktonic foraminifera (*G. ruber*, *G. sacculifer*, and *O. universa*). All ages were corrected for ^{13}C, and ^{14}C ages were converted to calendar years using the CALPAL 2007-Hulu software[3] and are reported as calendar years before present. We assume no regional deviation from the global reservoir effect of ~400 yr. The two nearest datasets from the Cocos (Keeling) Islands (411 ± 30 years)[4], and from Pelabuhanratu (362 ± 71 years) off West Java[5], suggest 400 years to be the most reasonable assumption. For the last deglaciation, evidence of larger deglacial reservoir ages in some upwelling regions[6,7] raises the possibility that there were also larger reservoir ages south of Java. If this were the case, a revised age model would

shift the observed events younger. However, a recently published study on a sediment core retrieved beneath the Java-Sumatra upwelling system[8] shows that the $\delta^{18}O$ of benthic foraminifera decreased simultaneously with the global benthic foraminifera stack record[9] and a benthic $\delta^{18}O$ record from the Timor Sea[10] during the last deglaciation. Since the age model of this core was based on radiocarbon dating on planktonic foraminifera[8], this resemblance suggests insignificant changes in the local carbon reservoir of the Java upwelling system during the last deglaciation. Moreover, new data from the Timor Sea[11] suggest insignificant changes in the reservoir ages during the last deglacial (100-200 years). According to the age model, sedimentation rates were about 21 cm kyr^{-1} during the last glacial and increased to ~27 cm kyr^{-1} during the last deglaciation. Sedimentation rates increased further during the early and middle Holocene (45 cm kyr^{-1}) and reached highest values during the late Holocene (~60 cm kyr^{-1}).

Table S1. Age control points of core GeoB 10053-7.
Conventional ages are converted to calendar ages using CALPAL2007-Hulu[3]. STD: Standard deviation.

Depth [cm]	**Lab-ID**	**^{14}C-age** [BP]	**± STD** [year]	**Cal. age (2σ, 95%)** [calBP (0=AD 1950]	**± STD** [year]
13	OS-61658	825	35	580-380	100
78	OS-71428	2170	15	1,770-1,610	80
138	OS-61659	2850	30	2,800-2,280	260
203	OS-71429	3800	20	3,720-3,600	60
263	OS-61665	4780	35	5,070-4,830	120
348	OS-66235	6340	40	6,890-6,650	120
393	OS-61666	7500	45	8,030-7,830	100
433	OS-71430	8240	25	8,680-8,560	60
483	OS-61616	9340	40	10,290-9,850	220
548	OS-61660	10550	40	12,050-11,610	220
578	UCI-68775	11795	30	13,200-13,360	80
598	OS-66236	12300	65	14,000-13,560	220
626	UCI-68776	12890	35	14,730-15,050	160
638	OS-61667	13100	50	15,430-15,030	200
650	UCI-68777	14210	40	16,920-17,080	80
663	OS-71431	15100	60	17,900-17,780	60
683	OS-66237	15950	85	18,810-18,610	100
713	OS-71432	17500	80	20,740-20,340	200
738	OS-61661	18450	80	21,750-21,390	180

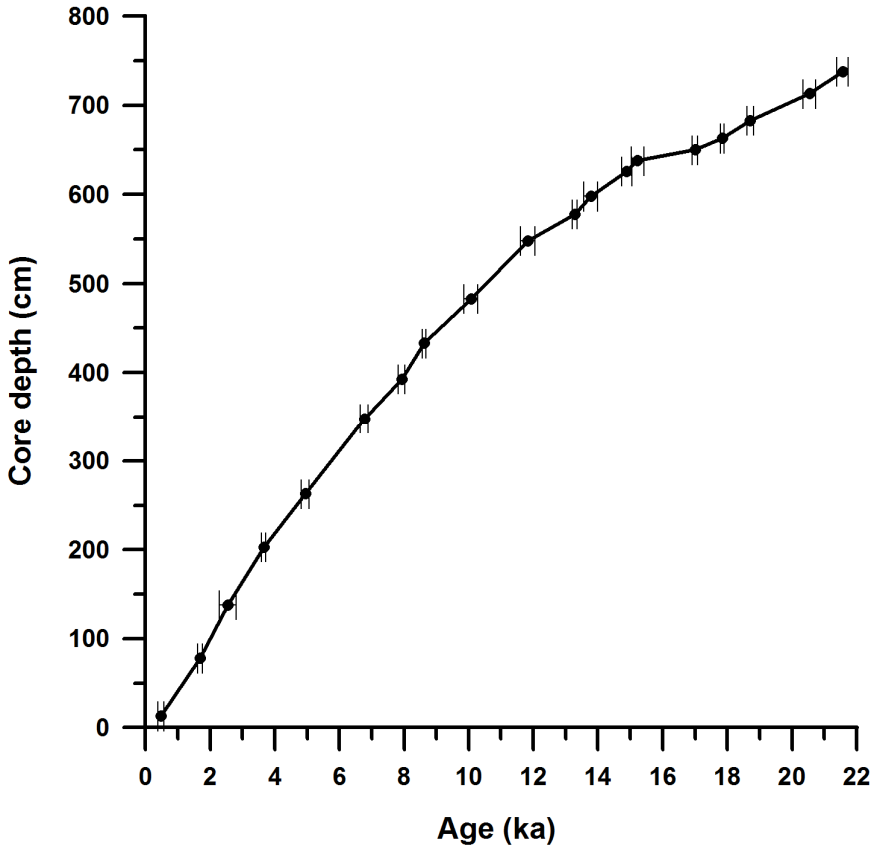

Figure S1. Age-depth relationship of core GeoB 10053-7.
Dots indicate radiocarbon dates with 2 sigma error bars.

Census counts and oxygen isotope analysis

A minimum of 300 planktonic foraminifera specimens from the size fraction >150 µm were counted in each of the 165 selected samples. The relative contribution of *G. bulloides* to total planktonic foraminiferal fauna was calculated and used as a measure of upwelling intensity.

A Finnigan MAT 251 mass spectrometer was used to measure the $\delta^{18}O$ composition of *G. ruber* sensu stricto and *G. bulloides* from 250-355 µm size-fraction. Approximately 5-20 individual tests were picked for each measurement. The isotopic composition of the carbonate sample was measured on the CO_2 gas evolved by treatment with phosphoric acid at a constant temperature of 75°C. For all stable isotope measurements a working standard was used, which has been calibrated against VPDB (Vienna Pee Dee Belemnite) by using the NBS 19 and 20 standards. Consequently, all isotopic data given here are relative to the PDB standard.

Analytical standard deviation is about ± 0.07‰ (Isotope Laboratory, Faculty of Geosciences, University of Bremen).

Terrigenous fraction analysis

XRF measurements were performed on the archive half of the splice core in 2 cm steps resulting in a total of 380 measurements with an average temporal resolution of 57 years per sample. Here we use the log-ratio between Ti and Ca as a measure for terrestrial input (Fig. S2-a). The significance and reliability of this method have been tested in a recent study[12]. We used Ti as the terrestrial end member since it lacks redox sensitivity, although other element ratios such as Fe/Ca are also highly correlated with Ti/Ca (Fig. S2-b). Likewise, we exclude changes in the biogenic Ca to account for the observed patterns in the Ti/Ca ratio, as other element ratios (Sr/Fe) show the same trends over the past 22,000 years (Fig. S2-c).

For bulk analyses, 148 samples averaging a 150-year temporal resolution per sample were freeze-dried and homogenized prior to processing. After decalcification of the samples with 6 N HCl, total organic carbon was obtained by combustion at 1050°C using a Heraeus CHN-O-Rapid elemental analyzer. Carbonate was calculated from the difference between total carbon (TC), measured with the CHN analyzer on untreated samples, and TOC, as:

$$CaCO_3 = (TC\text{-}TOC) * 8.33 \qquad (1)$$

$CaCO_3$ (TOC) contents ranged between 7% and 23% (0.9% and 2.4%) averaging about 14% (1.5%). All samples for opal analysis were freeze-dried and ground in an agate mortar. Opal was determined using a modified sequential leaching technique proposed by Müller and Schneider[13]. Opal contents ranged between 4% and 16% with an average value of 7.5%. The lithogenic fraction of the sediment was calculated by subtracting $CaCO_3$, opal, and TOC from total sediment, as:

$$Lithogenic = 100\text{-}(CaCO_3+opal+TOC) \qquad (2)$$

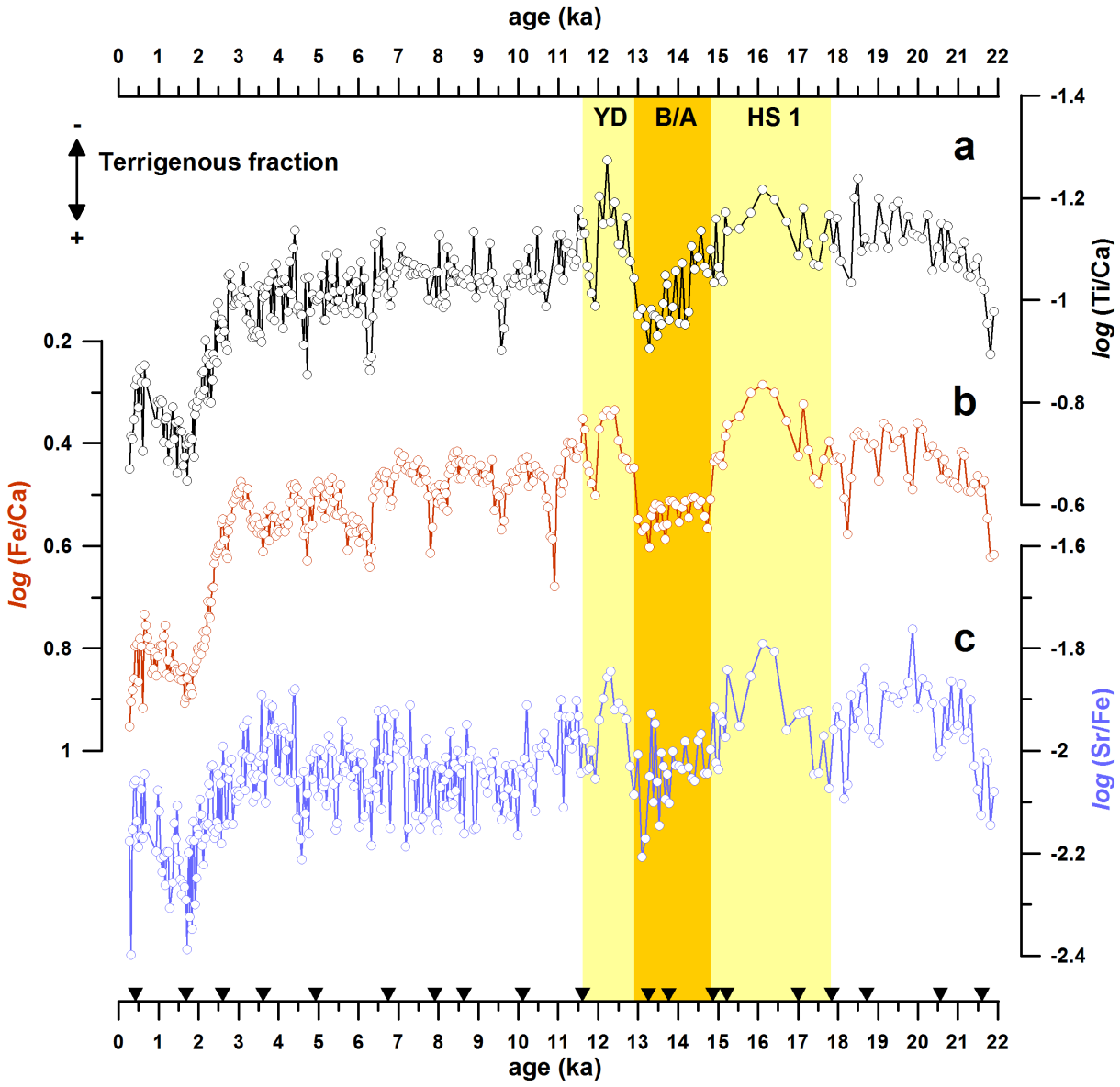

Figure S2. XRF data from core GeoB 10053-7.
Logarithmic ratio between Ti and Ca (a, black), Fe and Ca (b, red), and Sr and Fe (c, blue) showing a strong correspondence over the past 22,000 years (reversed scale). Triangles indicate age control points. HS1: Heinrich Stadial 1; B/A: Bølling-Allerød; YD: Younger Dryas.

Grain size analysis

Grain-size determination of 112 selected samples was performed with a Coulter Laser Particle Sizer LS200 on terrigenous material resolving grain-size spectra between 0.4 and 2000 µm in 92 size classes (Fig. S3). The terrigenous fraction was obtained by treating bulk sediment with 10 ml 10% hydrochloric acid (HCl) to remove $CaCO_3$, 10 ml 35% hydrogen

peroxide (H_2O_2) to remove organic matter, and 6 mg 1 N sodium hydroxide (NaOH) to remove biogenic opal. All samples were dispersed with 10 ml of 0.05 M sodium pyrophosphate ($Na_4P_2O_7 \cdot 10H2O$) prior to measurement. Median grain-sizes were calculated with the software GRADISTAT[14]after the method proposed by Folk and Ward[15].

Grain-size analyses of terrigenous fraction in two sediment cores from the SE Atlantic and the SE Pacific[16] showed that through the last glacial-interglacial cycle, wind-blown sediment fraction was coarser grained than the river-derived sediments due to the proximity of the source of the aeolian dust. Fluvial sediments are usually clay-fine silt sized, whereas aeolian dust is silt sized[16]. We therefore interpret the fine fraction of the terrigenous sediment as the river-derived, and the coarser grained fraction as the wind-blown end-members (Fig. S3).

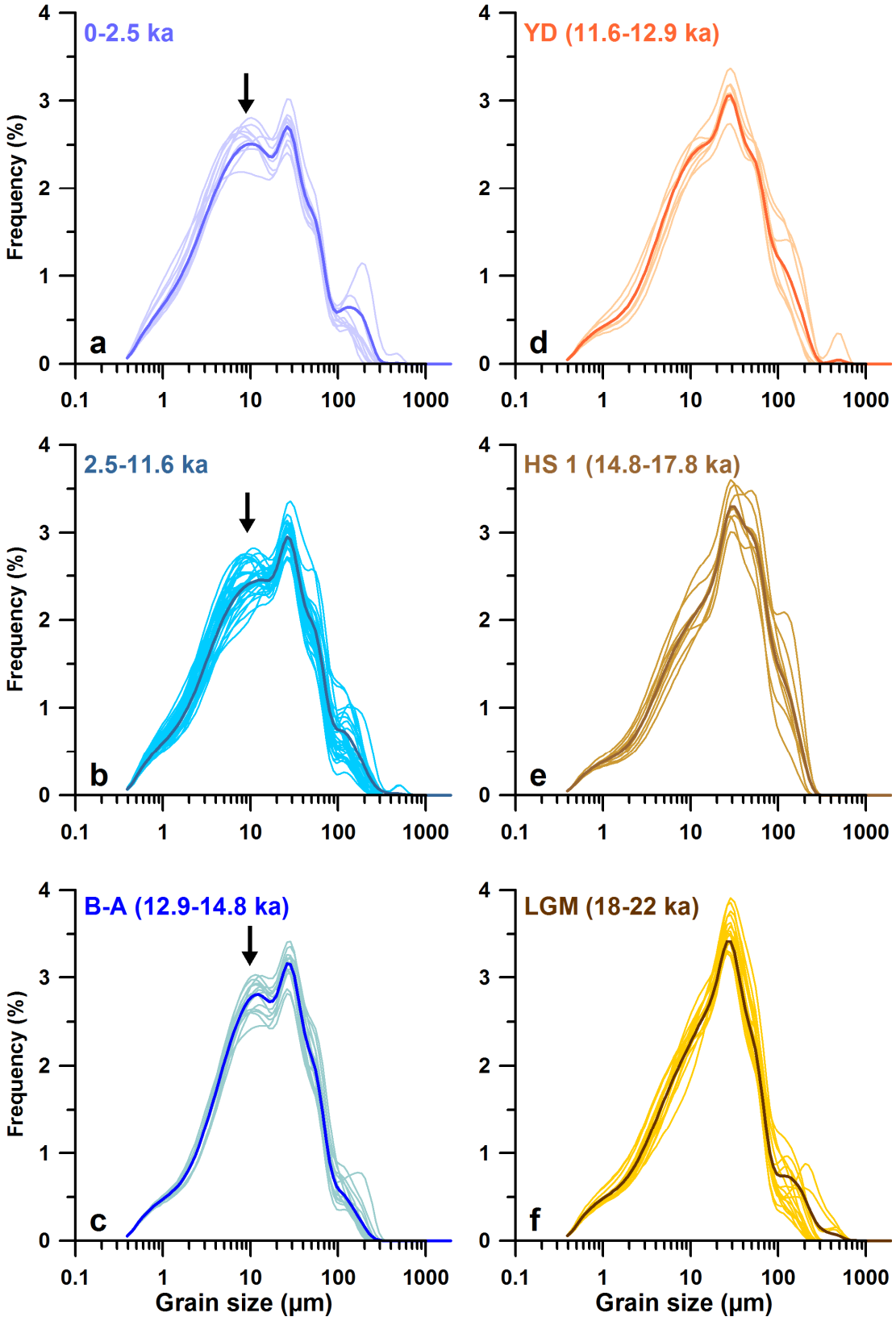

Figure S3. Grain-size data from core GeoB 10053-7.
Wet periods (a-c) are characterized by finer grained terrigenous fraction (see black arrows) whereas dries periods (d-f) show unimodal grain-size distributions of the coarser terrigenous fraction. Bold lines represent average grain-size distribution of the respective periods.

Modern calibration

Winter monsoon proxies:

The shell flux and chemistry of *G. ruber* and *G. bulloides* have been analysed in a sediment trap time-series off south Java (JAM1-3, Fig. S4)[17]. This study shows no seasonal preference in *G. ruber* fluxes over almost three years and suggests that this species records annual mean mixed-layer conditions between 0-30 m. In addition, the abundance-weighted SST value of *G. ruber* was calculated by assigning the in situ SST to each specimen and then averaged for the entire deployment period. The resulting SST (27.9°C) perfectly matches the measured SSTs averaged for 0-30 m water depth within the past 40 years (27.9°C, WOA05).

In contrast to *G. ruber*, about 90% of *G. bulloides* fluxes occur during the maximum upwelling between July and October (Fig. S4). In addition, net samples and CTD casts were deployed at the core site during the peak upwelling season (29.08.2005, *SO-184*). The vast majority of *G. bulloides* specimens were found at 0-50 m water depth, with their average shell $\delta^{18}O$ values (-2.22‰) converted to calcification temperature (22.5°C)[18] satisfactorily matching the contemporaneous CTD temperatures averaged for the same depth range (22.8°C, Fig. S5). As already shown for the Indian monsoon[19], *G. bulloides* relative contribution is one of the most powerful proxies for upwelling intensity and hence, seasonal changes in Australian-Indonesian (austral) winter monsoon intensity. The eligibility of this proxy for tracking upwelling intensity off S Java is also indicated in a sediment trap time-series[17] with highest relative abundances and total fluxes of *G. bulloides* occurring during the upwelling season (Fig. S4).

The strong correspondence between shell $\delta^{18}O$ of *G. bulloides* during the upwelling season in sediment traps (-2.42‰) and in the core-top at site 10053-7 (-2.47‰) suggests that downcore variability of these proxies should represent changes in the upwelling intensity that is inherently coupled to the austral winter monsoon intensity. Likewise, similar flux-weighted

$\delta^{18}O$ values of *G. ruber* in the sediment trap time-series (-2.93‰) and in the core-top at site 10053-7 (-2.85‰) suggest that annual mean conditions are well recorded by *G. ruber* in surface sediments off South Java[17]. From these findings we infer that downcore variations in shell chemistry of *G. ruber* (*G. bulloides*) represent past changes in the annual mean (winter) surface hydrography of the eastern Indian Ocean off South Java. Therefore, the difference between the $\delta^{18}O$ of *G. ruber* and *G. bulloides* ($\Delta^{18}O$) can be used to track changes in the winter upwelling intensity, whereby larger differences indicate stronger upwelling, and vice versa.

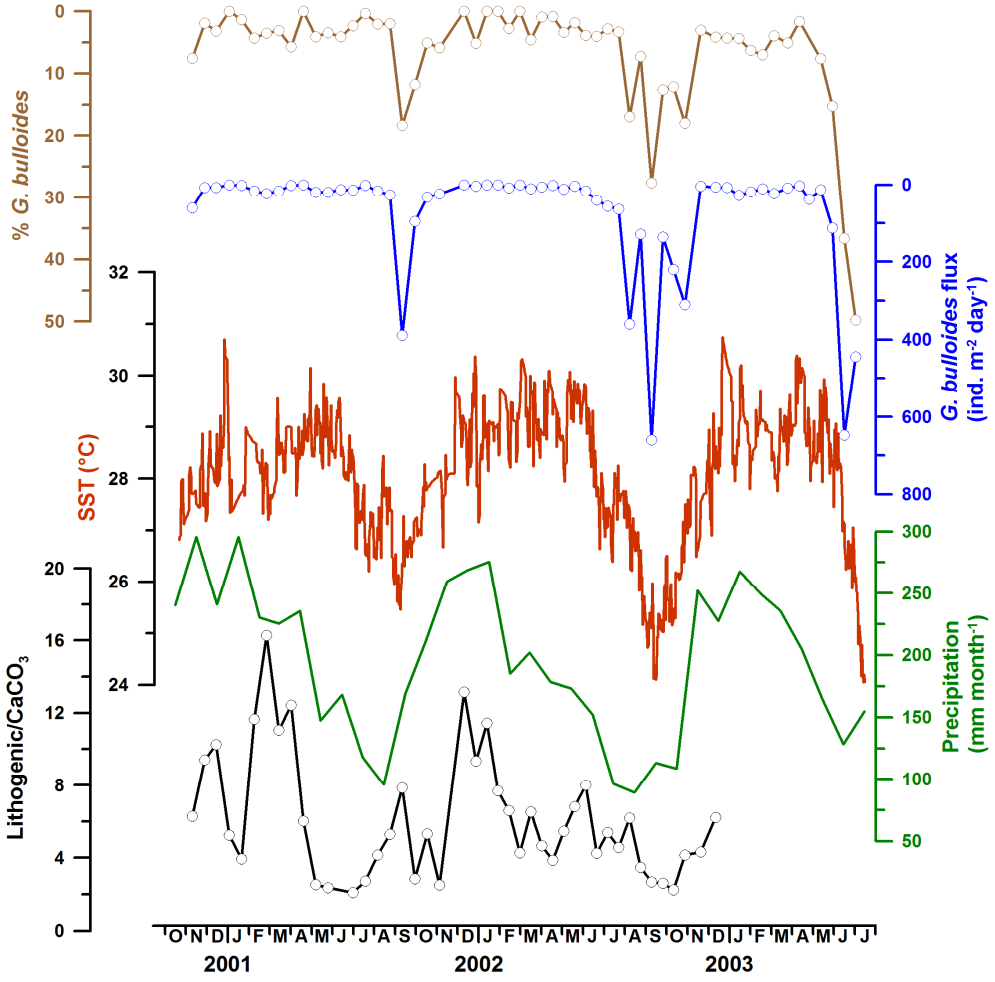

Figure S4. Climatologic data and measured parameters in the sediment trap time-series JAM1-3.
From top to bottom: Relative abundances (brown, reverse scale) and fluxes of *G. bulloides* (blue, reverse scale)[17]; Daily advanced very high resolution radiometer (AVHRR) SST data at the trap site (red, http://www.ncdc.noaa.gov); Precipitation over Indonesia (green, www.dwd.de); and lithogenic to calcium carbonate ratio (black)[22]. Note the pronounced monsoon-related cyclicity in all parameters.

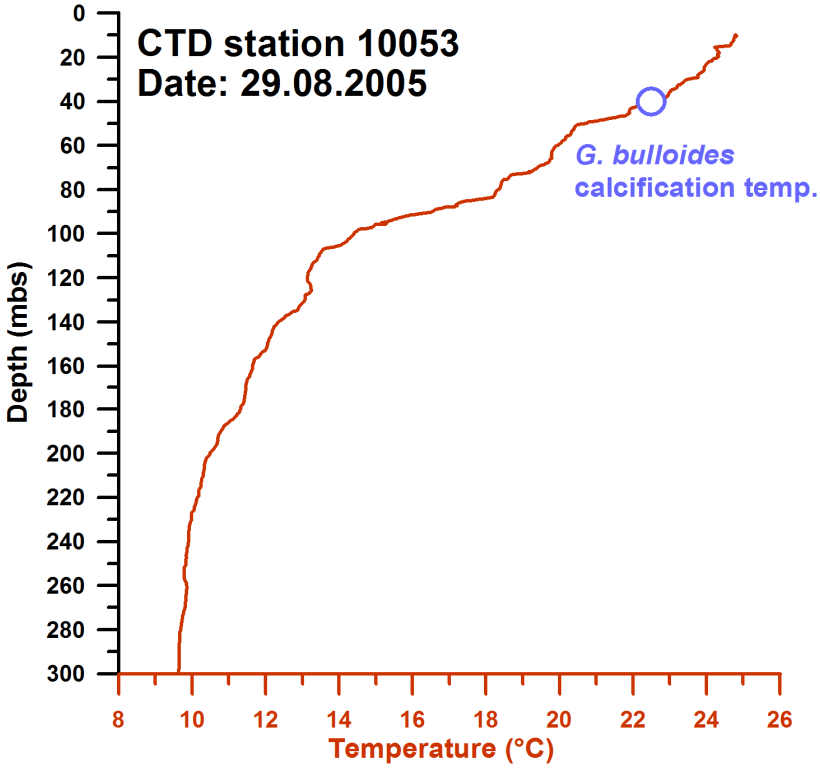

Figure S5. Habitat depth of *G. bulloides* in the study area.
Average calcification temperature derived from mean $\delta^{18}O$ values of *G. bulloides* found in multinet samples from the upper 50 m of water column (blue circle), and the temperature profile for the upper 300 m (CTD cast, red) at the same day. The size of the circle corresponds to the 1sigma error.

Summer monsoon proxies:

Today, precipitation over the core site is highest during the austral summer season[20] (December-March), when the ITCZ lies right above the study area (Figs. S6, S7-a). This strong monsoonal cyclicity of precipitation is mirrored in river discharge in eastern Java that is highest during summer and negligible during winter[21] (Fig. S7-b). Likewise, the ratio between the lithogenic particles and calcium carbonate in a sediment trap time-series off S Java displays the same, pronounced monsoonal cyclicity[22] (Fig. S4). Maximum values occur during the summer monsoon season between December and March, when onshore precipitation over the core site and river discharge in eastern Java are highest. Similar seasonality of precipitation, river discharge, and lithogenic fluxes in the water column suggests that the terrigenous fraction of the sediments off South Java is inherently coupled to

onshore precipitation during the austral summer monsoon. We therefore interpret downcore variations in the terrigenous fraction of GeoB 10053-7 as a measure of past changes in summer monsoon precipitation.

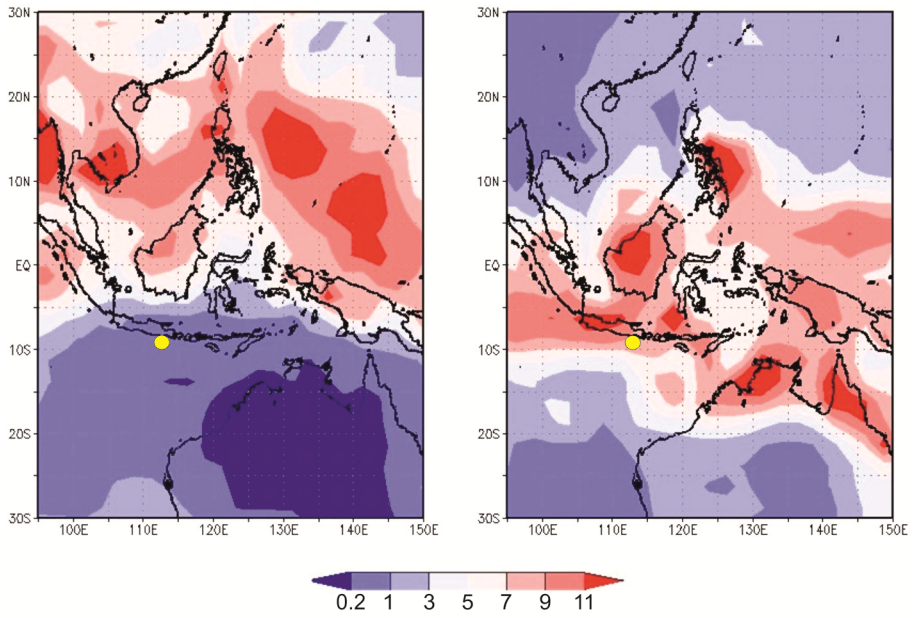

Figure S6. Monsoonal cyclicity of precipitation in the tropical Indo-Pacific.
Colour chart indicates seasonal precipitation for winter (a, July-September 2007) and summer (b, January 2007-March 2008) over Indonesia (http:// cics.umd.edu/~yin/GPCP) in mm day^{-1}. The yellow dot indicates the positions of the investigated core.

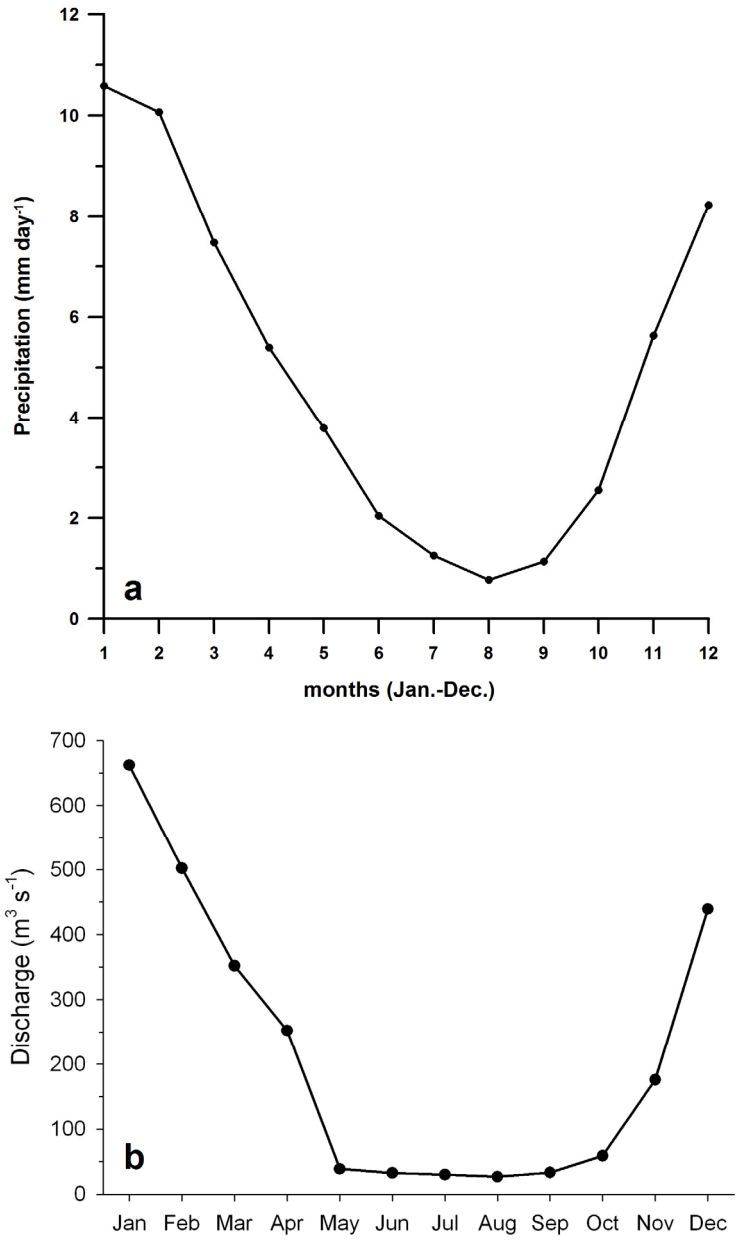

Figure S7. Average monthly precipitation and sediment discharge in E Java.
Average monthly precipitation (1979-2008) at the core site[20] (a) and average monthly discharge (1991-1996) of the Brantas River (Eastern Java) at Mojokerto[21] (b). Note that most of the discharge occurs during the wet summer monsoon period from December to March.

References

1 Hebbeln, D. *et al. Report and preliminary results of RV SONNE cruise SO-184, PABESIA, Durban (South Africa) - Cilacap (Indonesia) - Darwin (Australia), July 8th - September 13th, 2005*. (Universität Bremen, 2005).

2 Mohtadi, M. *et al.* Modern environmental conditions recorded in surface sediment samples off W and SW Indonesia: planktonic foraminifera and biogenic compounds analyses. *Marine Micropaleontology* **65**, 96-112 (2007).

3 Jöris, O. & Weninger, B. Extension of the ^{14}C calibration curve to ca. 40,000 cal BC by synchronizing Greenland $^{18}O/^{16}O$ ice core records and North Atlantic foraminifera profiles: A comparison with U/Th coral data. *Radiocarbon* **40**, 495-504 (1998).
4 Hua, Q. *et al.* Marine reservoir correction for the Cocos (Keeling) Islands, Indian Ocean. *Radiocarbon* **46**, 603-610 (2004).
5 Southon, J., Kashgarian, M., Fontugne, M., Metivier, B. & Yim, W. W.-S. Marine reservoir corrections for the Indian Ocean and Southeast Asia. *Radiocarbon* **44**, 167-180 (2002).
6 Bryan, S. P., Marchitto, T. M. & Lehman, S. J. The release of 14C-depleted carbon from the deep ocean during the last deglaciation: Evidence from the Arabian Sea. *Earth and Planetary Science Letters* **298**, 244-254, doi:DOI: 10.1016/j.epsl.2010.08.025 (2010).
7 Marchitto, T. M., Lehman, S. J., Ortiz, J. D., Fluckiger, J. & van Geen, A. Marine Radiocarbon Evidence for the Mechanism of Deglacial Atmospheric CO2 Rise. *Science* **316**, 1456-1459, doi:10.1126/science.1138679 (2007).
8 Mohtadi, M. *et al.* Late Pleistocene surface and thermocline conditions of the eastern tropical Indian Ocean. *Quaternary Science Reviews* **29**, 887-896 (2010).
9 Lisiecki, L. E. & Raymo, M. E. A Pliocene-Pleistocene stack of 57 globally distributed benthic $\delta^{18}O$ records. *Paleoceanography* **20**, PA1003, doi:1010.1029/2004PA001071 (2005).
10 Xu, J., Holbourn, A., Kuhnt, W., Jian, Z. & Kawamura, H. Changes in the thermocline structure of the Indonesian outflow during Terminations I and II. *Earth and Planetary Science Letters* **273**, 152-162 (2008).
11 Sarnthein, M., Grootes, P. M., Holbourn, A., Kuhnt, W. & Kühn, H. Tropical warming in the Timor Sea led deglacial Antarctic warming and atmospheric CO_2 rise by more than 500 yr. *Earth and Planetary Science Letters* **302**, 337-348, doi:10.1016/j.epsl.2010.12.021 (2011).
12 Weltje, G. J. & Tjallingii, R. Calibration of XRF core scanners for quantitative geochemical logging of sediment cores: Theory and application. *Earth and Planetary Science Letters* **274**, 423-438 (2008).
13 Müller, P. J. & Schneider, R. An automated leaching method for the determination of opal in sediments and particulate matter. *Deep-Sea Research I* **40**, 425-444 (1993).
14 Blott, S. J. & Pye, K. Gradistat: a grain-size distribution and statistics package for the analysis of unconsolidated sediments. *Earth Surface Processes and Landforms* **26**, 1237-1248 (2001).
15 Folk, R. L. & Ward, W. Brazos River bar: a study in the significance of grain size parameters. *Journal of Sedimentary Petrology* **27**, 3-26 (1957).
16 Stuut, J.-B. W. & Lamy, F. Climate variability at the southern boundaries of the Namib (southwestern Africa) and Atacama (northern Chile) coastal deserts during the last 120,000 yr. *Quaternary Research* **62**, 301-309 (2004).
17 Mohtadi, M. *et al.* Low-latitude control on seasonal and interannual changes in planktonic foraminiferal flux and shell geochemistry off south Java: A sediment trap study. *Paleoceanography* **24**, PA1201, doi:1210.1029/2008PA001636 (2009).
18 Bemis, B. E., Spero, H. J., Bijma, J. & Lea, D. W. Reevaluation of the oxygen isotopic composition of planktonic foraminifera: Experimental results and revised paleotemperature equations. *Paleoceanography* **13**, 150-160 (1998).
19 Gupta, A. K., Anderson, D. M. & Overpeck, J. T. Abrupt changes in the Asian southwest monsoon during the Holocene and their links to the North Atlantic Ocean. *Nature* **421**, 354-357 (2003).

20 Xie, P. & Arkin, P. A. Analyses of Global Monthly Precipitation Using Gauge Observations, Satellite Estimates, and Numerical Model Predictions. *Journal of Climate* **9**, 840-858 (1996).
21 Jennerjahn, T. C. *et al.* Biogeochemistry of a tropical river affected by human activities in its catchment: Brantas River estuary and coastal waters of Madura Strait, Java, Indonesia. *Estuarine, Coastal and Shelf Science* **60**, 503-514 (2004).
22 Rixen, T. *et al.* ENSO-driven carbon see saw in the Indo-Pacific. *Geophysical Research Letters* **33**, L07606, doi:07610.01029/02005GL024965 (2006).